Dopant-free back contacted silicon solar cells with an efficiency of 22.1%

Weiliang Wu[1,2], Wenjie Lin[1], Sihua Zhong[2], Bertrand Paviet-Salomon[3], Matthieu Despeisse,[3] Quentin Jeangros[2], Zongcun Liang[1,4], Hui Shen*[1,4], Mathieu Boccard*[2] and Christophe Ballif[2,3]

[1] Institute for Solar Energy Systems, School of Physics and State Key Laboratory of Optoelectronic Materials and Technologies, Sun Yat-Sen University (SYSU), Guangzhou, China.

[2] Photovoltaics and Thin Film Electronics Laboratory, Institute of Microengineering, École Polytechnique Fédérale de Lausanne (EPFL), Rue de la Maladière 71b, CH-2000 Neuchâtel, Switzerland.

[3] Centre Suisse d'Électronique et de Microtechnique (CSEM), PV-Center, Rue Jaquet-Droz 1, CH-2002 Neuchâtel, Switzerland.

[4] Shunde-SYSU Institute for Solar Energy, Shunde, China .

* Corresponding author: H.S. (shenhui1956@163.com); M.B. (mathieu.boccard@epfl.ch)

ABSTRACT

Contact recombination at the interface between the absorber material and the electrode interface is one of the most pressing issues limiting most photovoltaic technologies. Inserting a thin-film to prevent recombination while ensuring loss-free carrier extraction is a widely investigated route to fulfill this task. The multilayer films that include a low work-function metal such as calcium or magnesium simultaneously reduces contact recombination and resistance of the electron selective contact capped with an aluminum or silver electrode. Our results indicate that not only the metal in direct contact with the dielectric, but also the second capping metal is a crucial element of the contact stack. Although the exact mechanism is still unclear, low-work-function metals appear to perform better. We then apply the contact stack devised with these novel insights (1.5 nm MgF_x/20 nm Mg/100 nm Al) and MoO_x as well to dopant-free multilayer back contact (MLBC) solar cells to achieve an efficiency of 22.1% with an aperture area of 4.5 cm^2 by the directional evaporation for the patterning.

Keywords: electron-selective contact; dopant-free; solar cells; back contact; multilayer films.

1. Introduction

Silicon heterojunction back contact (HBC) solar cells have recently demonstrated an impressive efficiency of 26.6 % on industrial wafer[1]. In such device, the doped a-Si:H (n) and a-Si:H (p) layers require complex deposition processes including low deposition rates, high capex and toxic gases.[2-5] Such high efficiency also relies on a detailed optimization to finely tune the composition and interdependency of all involved layers. On the other hand, dopant-free asymmetric carrier selective contact concept has been applied in two-sides solar cells to completely replace doped a-Si:(n) and a-Si:(p) layers with dopant-free materials such as transition metal oxides (TMOs), alkaline metal compounds, and organic polymers, recently achieving promising efficiencies above 20%.[6,7] Dopant-free carrier selective contacts have also been successfully applied in interdigitated back contact structures to avoid the front parasitic absorption and the processing constraints arising from the doped a-Si layers in HBC solar cells. The state-of-the-art efficiency of dopant-free IBC solar cells has been exceeding 19%[7,8]. Materials used so far as dopant-free carrier-selective contacts include hole-selective molybdenum oxide (MoO_x)[7,9-14], tungsten oxide (WO_x)[10,14], vanadium oxide (V_2O_x)[12,14], chromium oxide (CrO_x)[10,13-17], and electron-selective lithium fluoride (LiF_x)[6,18], tantalum oxide (TaO_x)[19], titanium dioxide (TiO_2)[20], magnesium fluoride (MgF_x)[21], magnesium oxide (MgO_x) [22], magnesium (Mg)[23], calcium (Ca)[24]. The key issue is to optimize the trade-off between contact resistivity and recombination of charge carriers at the hole- and electron- selective contacts[2]. Recently, a promising strategy to improve the selectivity of contacts is to employ multilayer films such as TiO_2/Ca[25], Al_2O_3/TiO_2/Mg and TaO_x/Mg[19] covered with Al as electrode, which has been demonstrated to yield a reduced contact resistivity and recombination losses at the hetero-interface with c-Si, presumably with little influence from this second capping metal.

In this article, we evidence the role of both capping metals on the effectiveness of dopant-free electron-selective contacts. We show the negative influence on the cell photovoltaic performance induced by a non-optimized capping contact metal electrode, even on top of a 20-nm-thick Mg layer. In order to reveal the mechanism of the Mg/metal contact interfacial properties, the morphology and element distribution of metal/magnesium contact interface are observed by scanning transmission electron microscopy (STEM). We apply these learnings in solar cell devices using a simple two-step thermal evaporation process to form the electron and hole contacts of dopant-free back-contacted silicon solar cells, demonstrating an efficiency of 22.1%.

2. Results and discussion

Figure 1a shows the diagram of front junction solar cell used in this study. An MgF_x/Mg/metal stack was used as electron-selective contact. To investigate the influence of the work function (W_F) of this second metal layer on the effectiveness of the contact, we select five groups of metals with different W_F, Mg, Al, Ag, Cu and Au. This second metal layer of 100 nm was deposited on top of the 20 nm Mg layer after a vacuum break of 30 min.

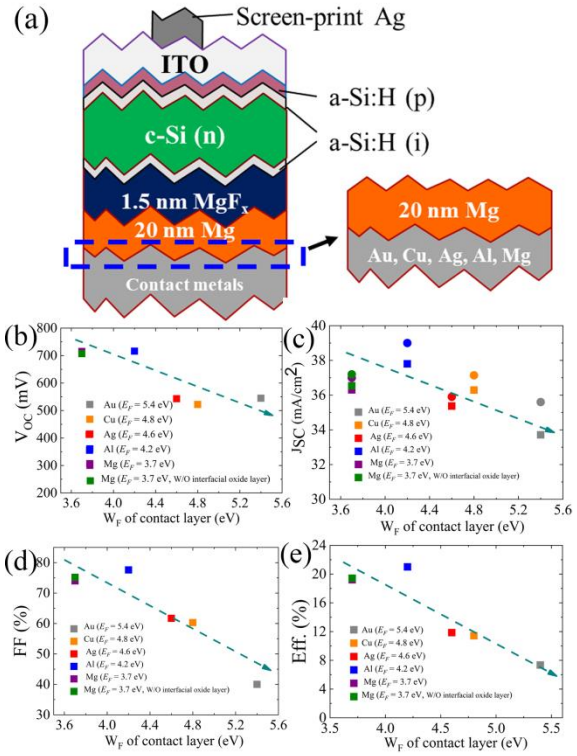

Figure 1. Effect of contact metal W_F on photovoltaic performance of the front junction solar cells. a, Sketch of front junction solar cells with MgF_x/Mg as electron contact covered with different W_F metals. **b-e,** Main parameters from the light *J-V* characteristics of devices with varying W_F metals covering on Mg surface. The dotted circle in **c** is the integrated J_{SC} from *EQE*.

Fig 1b - e shows the effect on V_{OC}, *FF*, J_{SC} and η of increasing W_F of contact metals. A decrease of performance for increasing W_F is seen. For Au, Cu and Ag, which are contact layers featuring the relatively high vacuum W_F of 5.4 eV, 4.8 eV and 4.6 eV[26], respectively, low V_{OC} and *FF* values below 600 mV and 65% are obtained, whereas for Al and Mg contact layers featuring the low vacuum W_F, high V_{OC} and *FF* values over 700 mV and 75% are achieved. This is reflected in a fast decrease of η from 21% to 8% with the increasing W_F of the contact metal layer from 3.7 eV to 5.4 eV. Note that comparing a stack of 20 nm Mg (exposed to air) + 100 nm Mg, to a single-deposition 120 nm Mg without breaking vacuum, both contacts show similar device performance which indicates that a possible interfacial MgO_x layer (formed in air) does not influence the performance of devices. As shown in Fig 1c, integrated J_{SC} from *EQE* agrees well with that obtained directly from the light *J-V* supporting the accuracy of the value, as detailed in the Figure S1.

To elucidate whether the V_{OC} drop observed in Fig. 1b when increasing the W_F of the metal layer is caused by a recombination increase, photoluminescence (PL) images from the front side of solar cells shown in Fig. 2a-e. These indicate a clear loss of intensity when increasing the capping-metal W_F, consistently with an increase of recombination. A drop in infrared *IQE* is also observed upon increasing the W_F of the capping metal (Fig. 2f), which strengthens the hypothesis that this V_{OC} loss is due to an increased recombination at the rear side.[27] This is unexpected since the 20-nm-thick Mg layer between the studied capping metal and MgF_2 layer is expected to screen entirely the electrical effects of the capping metal. We will discuss the possible mechanisms using microscopy images showing the interfacial microstructure in the next section.

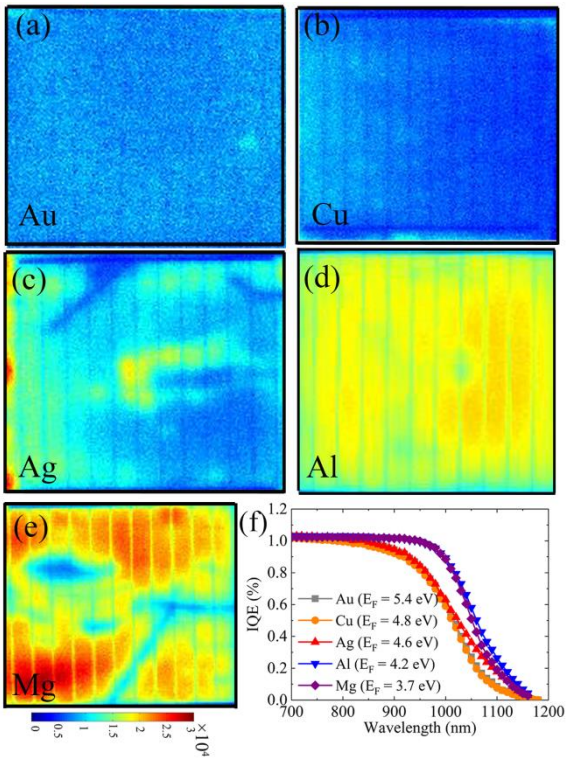

Figure 2. Cell recombination measurement. a-e, Photoluminescence (PL) images of solar cells with different W_F of contact metals that contain Au, Cu, Ag, Al and Mg at 1-sun photon flux. **f,** IQE curves of solar cells.

In order to further observe the interfacial structures and chemical elements after MgF_x/Mg/Al evaporation, we performed STEM high-angle annular dark-field (HAADF) imaging coupled with energy-dispersive X-ray spectroscopy (EDX) as shown in Fig 3. The STEM HAADF micrograph and corresponding Al, Mg, O, F, and Si EDX maps are shown in Fig 3a. Oxygen with high concentration is observed in the whole Mg layer. This may be generated from the non-dense Mg layer and the transfer from the focused ion beam (FIB) to the STEM, yet it is quite plausible that oxidation happened during the air exposure between both metal layer depositions. Interestingly, the low concentration fluoride elements are also distributed in the whole cross-section surface, and not only at the MgF_x layer position. These observations evidence that strong diffusion occurs in the Mg layer.

Fig 3b-c show STEM HAADF micrograph and corresponding Mg, F, O and Si EDX and EDS maps focusing on the interface. We observe some Mg signal on the a-Si:H side of the MgF_x layer, likely indicating that some Mg diffused through the latter layer during the metal evaporation. Note also that the oxidation of the MgF_x layer should significantly improve its conductivity[25,28] and also improve the *FF* of the device. Interestingly, the Mg diffusion into the a-Si:H (i) does not seem to impact passivation drastically, as seen from the good V_{OC} and PL images obtained with the MgF_x/Mg/Al stack. Also, comparison of a device using such a contact to a similar device without the Mg layer (MgF_x/Al contact stack) indicates a better Voc (716 mV compared to 707 mV) and overall performance (21.0% compared to 19.8%) for the device with the Mg layer. No Al is seen to migrate through the Mg layer from this microscopy study. Yet, seeing the O and F signal in the Mg

layer, it cannot be ruled out that little amounts do migrate, at least locally, not enough to be detected in EDS, but in sufficient quantity to have a strong influence on the electronic quality of the contact. Such effect would be highly detrimental to passivation and carrier-selectivity in the case of high-WF metals (Au, Cu and Ag) but of lesser effect for Al and unnoticed for Mg, and could be a reason for the effect of the metal on the solar cell performance.

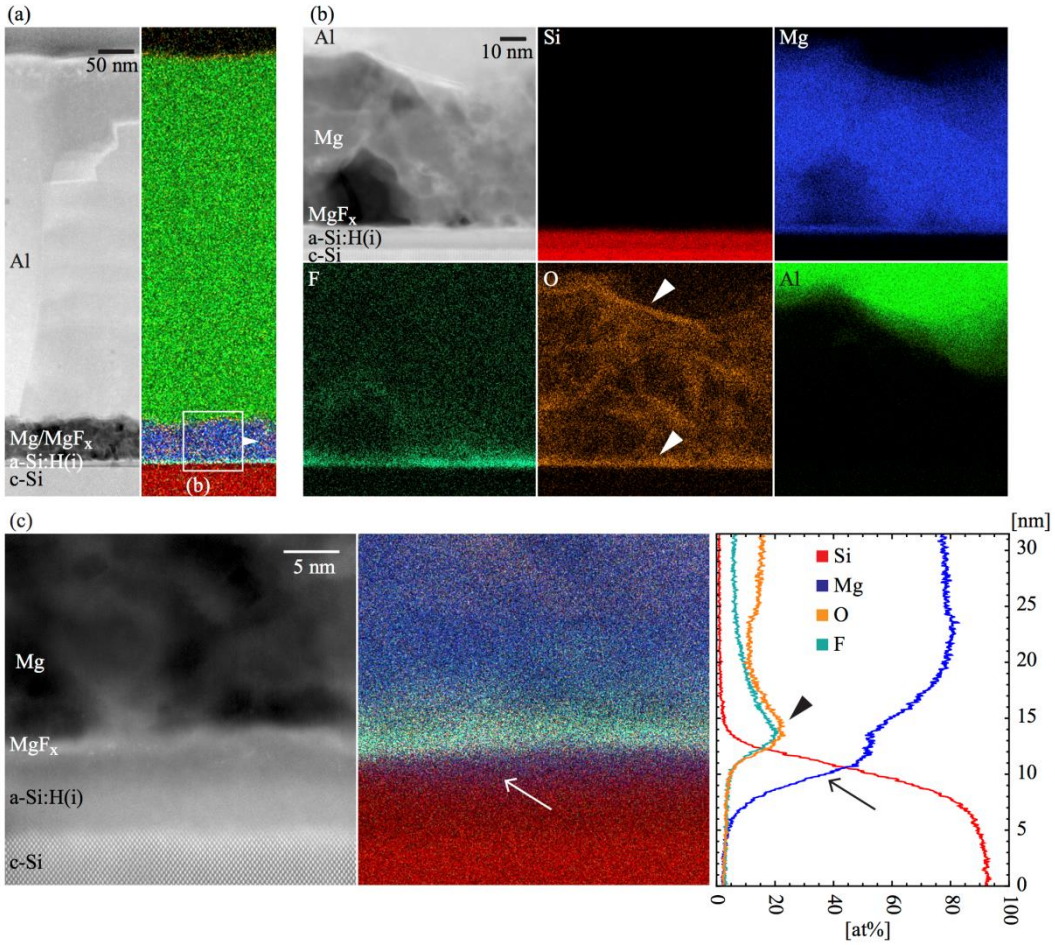

Figure 3. The multilayer electron selective contact microstructure. a, STEM HAADF image and corresponding EDX map of the full electron carrier-selective stack microstructure. **b,** Higher magnification STEM HAADF image of the contact alongside the corresponding EDX maps of the Si K, Mg K, F K, O K and Al K ionization edges. **c,** High-resolution STEM HAADF image and corresponding EDX map and atomic concentration line profile across the MgF_2 interlayer. The EDX data was quantified using the Bruker Esprit software using the Cliff-Lorimer method[29]. Arrowheads indicate that the bottom and top interface of the Mg layer is oxidized, while arrows highlight the presence of a Mg layer in between the MgF_x and a-Si:H(i) layers.

Fig 4a shows a sketch of the MLBC solar cell fabricated using this low-contact-recombination and efficient electron-transport multilayer of 1.5 nm MgF_x/ 20 nm Mg/ 100 nm Al. A 6-nm-thick a-Si:H (i) layer was first deposited by plasma enhanced chemical vapor deposition (PECVD) on both

sides of the wafer. A stack composed of 50-nm-thick SiN_x (n = 1.96) layer deposited by PECVD capped by an evaporated 90-nm-thick MgF_2 layer was then deposited on the front side to ensure excellent front surface passivation and good light in-coupling. The detailed fabrication process is shown in the Figure S2; a two-metal-mask patterning process was then employed to fabricate rear contacts of the MLBC solar cell in lieu of the usual photolithography, reducing the patterning steps for the p- and n- contact into two steps. We measured the cells with the 3 cm × 1.5 cm designated area using a mask excluding the busbar area.

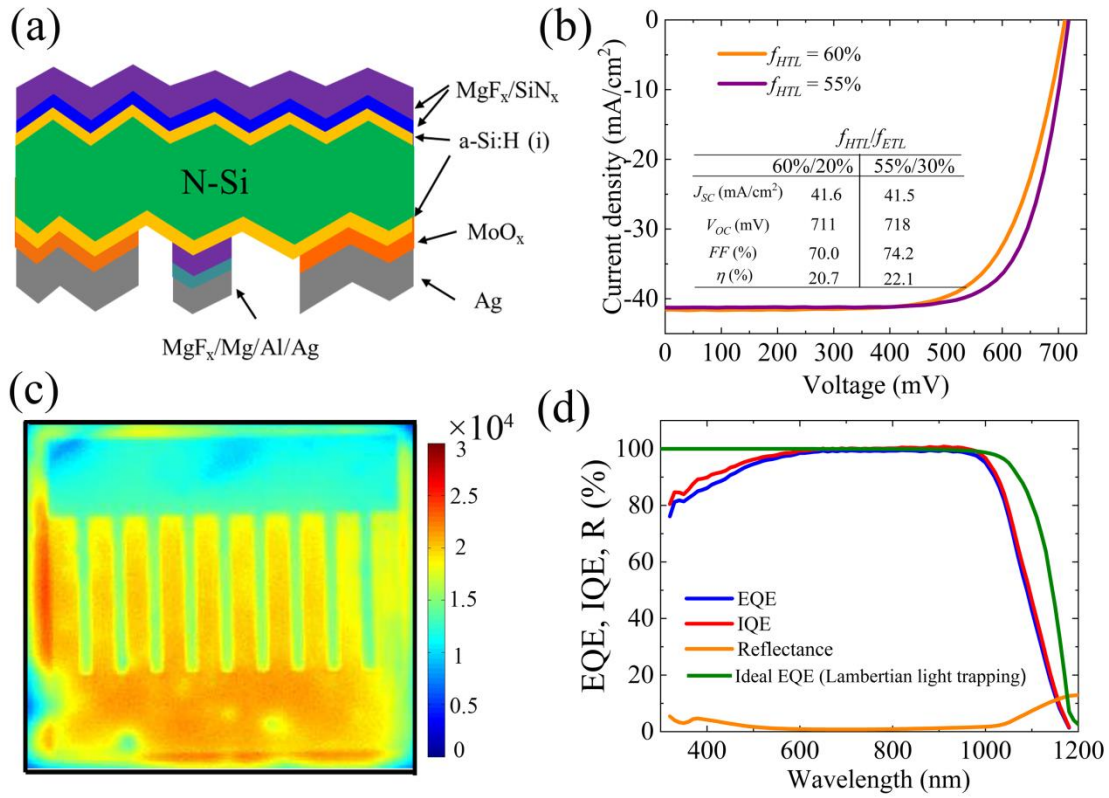

Figure 4. Design and performance of the MLBC solar cell. a, Diagram of MLBC solar cells featuring MoO_x/Ag and MgF_x/Mg/Al/Ag as hole- and electron-selective contacts, respectively. **b,** One sun *J-V* curves of MLBC solar cells with the electron-selective-contact-area fraction of 20% and 30%, respectively. **c,** Photoluminescence (PL) images of the MLBC solar cell with electron-selective-contact-area fraction (f_{ETL}) of 30%. **d,** External quantum efficiency (*EQE*), reflectance *(R)* and internal quantum efficiency (*IQE*) of the same cell.

Fig 4b shows the measured light *J-V* curves of MLBC solar cell with the electron selective contact fraction of 30% and 20% in order to balance the influence of back contact cell geometry on contact resistivity and contact recombination. We observe a lower series resistance (R_S) loss for the larger electron-selective-contact-area fraction of 30%. Thicknesses of a-Si:H (i) and MgF_x were carefully optimized to allow maximal efficiency (Figure S3, Figure S4 and Table S1). Table S2 summarizes the current state of the art of dopant-free silicon solar cells, we limit it with efficiency higher than 20.7%. A best efficiency of 22.1% was achieved with V_{OC} and *FF* values of 718 mV and 74.2%, respectively. Due to the relatively thin Ag layer (800 nm) used in these MLBC solar cells, series resistance is still large, partly causing the relatively low *FF*. The pseudo *FF* (*pFF*: *FF*

excluding R_S power loss) of 84.2% and pseudo efficiency (efficiency excluding R_S power loss) of 25.1% are however indicative of a high potential for the approach (see Figure S5 and Figure S6 for further MLBC solar cell characterization). Fig 4c shows the PL images of the MLBC solar cell indicating that surface recombination is larger for the electron-selective-contact area compared to the hole-selective-contact area. As can be seen in Fig. 4d, high EQE and low reflection can be attained on the whole visible part of the spectrum.

The J_{SC} value of 41.5 mA/cm^2 is 2.8 mA/cm^2 lower than the theoretical limit J_{SC} = 44.3 mA/cm^2 of c-Si (n) solar cell for a thickness of 240 μm and N_{dop} of 1 × 10^{16} cm^{-3}.[30] The ideal *EQE* is calculated for the same wafer thickness (240 μm) with no front side reflectance using ideal Lambertian light trapping and recombination of solar cell[31]. The loss in the short wavelength part corresponding to the wavelength integration range between 350 nm and 600 nm is mainly caused by the front-surface parasitic absorption of the a-Si:H (i) layer. The J_{SC} losses in the long wavelength ranging from 1000 to 1200 nm are mostly caused by the parasitic absorption of the a-Si:H (i)/MoO_x/Ag and MgF_x/Mg/Al/Ag layers. Reducing the rear-side parasitic absorption would require inserting a thick-enough low-refractive index layer between the silicon wafer and the metal layers,[32] yet the contact-resistance values for both contacts do not allow local contact without drastic series resistance losses, making such approach non-viable for this device.

3. Conclusion

In this work we have shown the influence of metal capping layer on MgF_x/Mg electron-selective contact stacks. The low-recombination and efficient-electron-transport multilayer films of 1.5 nm MgF_x/20 nm Mg /100 nm Al as electron-selective contacts is applied in the proof-of-concept of dopant-free MLBC solar cell with high conversion efficiency over 22.1%. This represents a significant improvement on the state of the art for dopant-free IBC. Further improvements rely on increasing the infrared response by introducing an optical spacer between the metal and the silicon wafer, as well as improving the stability of the electron-selective contact stack. Overcoming these limitations is expected to require the development of alternative materials, but this would allow very high efficiency for dopant-free silicon solar cells and possibly industrial adoption.

4. Methods section

4.1 Fabrication and characterization of solar cells.

N-type (100) oriented float-zone silicon wafers (2.5 Ω cm, 250 μm) were used for all the device fabrications in this study. The Si wafers were etched in potassium hydroxide to obtain a random-pyramid surface texture. After chemical cleaning, the wafers were dipped in 1% hydrofluoric acid for 1 min to remove the surface native oxide. Thin intrinsic a-Si:H films were then deposited by plasma-enhanced chemical vapor deposition (PECVD) on both sides of the wafer to enable high-quality surface passivation. For 2-side contacted devices, an a-Si:H(p) layer deposited with PECVD was used on the front side of the wafer. ITO was deposited by reactive sputtering through shadow masks to define the 2 × 2 cm^2 cell area. A low-temperature silver paste was screen-printed to form the front grid, followed by curing for 20 minutes at 210 °C). The electron selective contact was realized by thermal evaporation of 1.5 nm MgF_x/20 nm Mg layer at the rear side without breaking the vacuum. After breaking the vacuum, the Mg surface was evaporated with different W_F contact metals including Au, Cu, Ag, Al and Mg as electrode.

For back-contacted devices, a DARC (double antireflection coating) film consisting of 50 nm SiN_x followed by 90 nm thick MgF_x was deposited on the front side, by PECVD at a substrate temperature of 200 °C for the SiN_x film, and room-temperature thermal evaporation for the MgF_2 film. A metal mask patterning process was employed in the present study to fabricate IBC solar cells featuring hole- and electron-selective contacts in lieu of the usual photolithography. For the rear-side contacts, an 8-nm-thick MoO_x and 800-nm-thick Ag layers were applied by thermal evaporation conducted at a room temperature with a deposition rate of about 0.2 - 0.5 Å/s at a base pressure of 1.0×10^{-5} Torr with in-situ metal mask 1. The 1.5 nm MgF_x/ 20 nm Mg/35 nm Al / 800 nm Ag films were thermally evaporated onto the wafer substrate with the in-situ metal shadow mask 2. A precise alignment was obtained by this simple process, forming a uniform 200 μm gap between the MoO_x/Ag and MgF_x/Mg/Al/Ag contacts.

The light *J-V* behavior was measured under standard one-sun conditions (100 mW/cm^2, AM1.5 spectrum, 25℃) with a Wacom WXS-90S-L2 solar simulator, and the dark *J-V* behavior was also investigated. The External Quantum Efficiency (*EQE*) was conducted using a Solar Cell Quantum Efficiency Measurement System (in-house built setup). The J_{SC} of the cell was integrated by the *EQE*. The injection level dependent open-circuit voltage was measured by transient photo-conductance measurement (WCT-120, Sinton).

4.2 Material characterization.

For STEM observations, c-Si/a-Si:H(i)/MgF_x/Mg/Al layer stacks were deposited onto polished (100) oriented Fz wafers. The cross-section of c-Si/a-Si:H(i)/MgF_x/Mg/Al interfaces were obtained by a focused ion beam (FIB) lift-out technique in a Zeiss NVision 40 and observed by FEI Tecnai G2 F30 transmission electron microscopy (TEM) operating at 300 kV. The high-resolution HAADF micrographs were obtained in an image and probe Cs corrected FEI Titan Themis microscope, the system was operated at 200 kV with a beam current of about 100 pA. For HAADF imaging, the beam convergence semi-angle was set to 28 mrad and the camera length to 115 mm (corresponding to an HAADF detector collection semi-angle of 55.5 to 200 mrad). The high-resolution TEM imaging coupled with EDX spectroscopy mapping maps were recorded with a beam current of 200 pA and a solid angle >0.7 srad, using four-quadrant silicon drift detectors.

Notes

The authors declare no competing financial interest.

Acknowledgements

This project has received funding from the European Union's Horizon 2020 research and innovation programme under Grant Agreement No. 727523 (NextBase). This work was supported by the National Natural Science Foundation (contract no. 61774173), the International Program for Ph.D. Candidates at Sun Yat-Sen University (grant no.02300-18827001), and the Jiangsu Collaborative Innovation Center of Photovoltaic Science and Engineering (grant no. SCZ1405500002).

Appendix A. Supporting information

Supplementary data associated with this article can be found in the online version.

References

[1] K. Yoshikawa, W. Yoshida, T. Irie, H. Kawasaki, K. Konishi, H. Ishibashi, T. Asatani, D. Adachi, M. Kanematsu & H. Uzu, *Solar Energy Materials & Solar Cells* 173 (2017).

[2] S. M. D. Nicolás, J. Coignus, W. Favre, J. P. Kleider & D. Muñoz, *Solar Energy Materials & Solar Cells* 115 (2013) 129-137.

[3] A. Tomasi, B. Paviet-Salomon, D. Lachenal, S. M. d. Nicolas, A. Descoeudres, J. Geissbühler, S. D. Wolf & C. Ballif, *IEEE Journal of Photovoltaics* 4 (2014) doi:10.1109/JPHOTOV.2014.2320586 1046-1054.

[4] B. Paviet-Salomon, A. Tomasi, A. Descoeudres, L. Barraud, S. Nicolay, M. Despeisse, S. D. Wolf & C. Ballif, *IEEE Journal of Photovoltaics* 5 (2015) 1293-1303.

[5] A. Tomasi, B. Pavietsalomon, Q. Jeangros, J. Haschke, G. Christmann, L. Barraud, A. Descoeudres, J. P. Seif, S. Nicolay & M. Despeisse, *Nature Energy* 2 (2017) 17062.

[6] J. Bullock, M. Hettick, J. Geissbühler, A. J. Ong, T. Allen, C. M. Sutterfella, T. Chen, H. Ota, E. W. Schaler & S. D. Wolf, *Nature Energy* 1 (2016) 15031.

[7] H. D. Um, N. Kim, K. Lee, I. Hwang, H. S. Ji & K. Seo, *Nano Letters* 16 (2016) 981-987.

[8] G. Masmitjà, P. Ortega, J. Puigdollers, L. G. Gerling, I. Martín, C. Voz & R. Alcubilla, *Journal of Materials Chemistry A* 6 (2018).

[9] M. Bivour, B. Macco, J. Temmler, W. M. M. Kessels & M. Hermle, *Energy Procedia* 92 (2016) 443-449.

[10] L. G. Gerling, S. Mahato, A. Morales-Vilches, G. Masmitja, P. Ortega, C. Voz, R. Alcubilla & J. Puigdollers, *Solar Energy Materials & Solar Cells* 145 (2015) 109-115.

[11] J. Geissbühler, J. Werner, S. M. D. Nicolas, L. Barraud, A. Hesslerwyser, M. Despeisse, S. Nicolay, A. Tomasi, B. Niesen & S. D. Wolf, *Applied Physics Letters* 107 (2015) 1433-1435.

[12] C. Battaglia, S. M. D. Nicolás, S. D. Wolf, X. Yin, M. Zheng, C. Ballif & A. Javey, *Applied Physics Letters* 104 (2014) 1-24.

[13] W. Wu, W. Lin, J. Bao, Z. Liu, B. Liu, K. Qiu, Y. Chen & H. Shen, *Rsc Advances* 7 (2017) 23851-23858.

[14] W. Wu, J. Bao, Z. Liu, W. Lin, X. Yu, L. Cai, B. Liu, J. Song & H. Shen, *Materials Letters* 189 (2017) doi:10.1016/j.matlet.2016.11.059 86-88.

[15]L. G. Gerling, G. Masmitja, C. Voz, P. Ortega, J. Puigdollers & R. Alcubilla, *Energy Procedia* 92 (2016) 633-637.

[16]W. Lin, W. Wu, Z. Liu, K. Qiu, L. Cai, Z. Yao, B. Ai, Z. Liang & H. Shen, *ACS applied materials & interfaces* (2018) doi:10.1021/acsami.8b02878.

[17]W. Lin, W. Wu, J. Bao, Z. Liu, K. Qiu, L. Cai, Z. Yao, Y. Deng, Z. Liang & H. Shen, *Materials Research Bulletin* (2018).

[18]J. Bullock, P. Zheng, Q. Jeangros, M. Tosun, M. Hettick, C. M. Sutter‐Fella, Y. Wan, T. Allen, D. Yan & D. Macdonald, *Advanced Energy Materials* 6 (2016).

[19]Y. Wan, S. K. Karuturi, C. Samundsett, J. Bullock, M. Hettick, D. Yan, J. Peng, P. R. Narangari, S. Mokkapati & H. H. Tan, *Acs Energy Letters* 3 (2018).

[20]J. Cui, T. Allen, Y. Wan, J. Mckeon, C. Samundsett, D. Yan, X. Zhang, Y. Cui, Y. Chen & P. Verlinden, *Solar Energy Materials & Solar Cells* 158 (2016) 115-121.

[21]Y. Wan, C. Samundsett, J. Bullock, T. Allen, M. Hettick, D. Yan, P. Zheng, X. Zhang, J. Cui & J. Mckeon, *ACS applied materials & interfaces* 8 (2016) 14671-14677.

[22]Y. Wan, C. Samundsett, J. Bullock, M. Hettick, T. Allen, D. Yan, J. Peng, Y. Wu, J. Cui & A. Javey, *Advanced Energy Materials* 7 (2017).

[23]Y. Wan, C. Samundsett, D. Yan, T. Allen, J. Peng, J. Cui, X. Zhang, J. Bullock & A. Cuevas, *Applied Physics Letters* 109 (2016) 024107-014677.

[24]T. G. Allen, J. Bullock, P. Zheng, B. Vaughan, M. Barr, Y. Wan, C. Samundsett, D. Walter, A. Javey & A. Cuevas, *Progress in Photovoltaics Research & Applications* 25 (2017) n/a-n/a.

[25]T. G. Allen, J. Bullock, Q. Jeangros, C. Samundsett, Y. Wan, J. Cui, A. Hessler‐Wyser, S. D. Wolf, A. Javey & A. Cuevas, *Advanced Energy Materials* 7 (2017) 1602606.

[26]M. Bivour, C. Reichel, M. Hermle & S. W. Glunz, *Solar Energy Materials & Solar Cells* 106 (2012) 11-16.

[27]R. Brendel, M. Hirsch, R. Plieninger & J. J. H. Werner, 43 (1996) 1104-1113.

[28]H. Tong, Z. Yang, X. Wang, Z. Liu, Z. Chen, X. Ke, M. Sui, J. Tang, T. Yu & Z. Ge, *Advanced Energy Materials* (2018) 1702921.

[29]G. Cliff & G. W. Lorimer, *J Microscopy* 103 (2011) 203-207.

[30]A. Richter, M. Hermle & S. W. Glunz, *IEEE Journal of Photovoltaics* 3 (2013) 1184-1191.

[31]K. Yoshikawa, H. Kawasaki, W. Yoshida, T. Irie, K. Konishi, K. Nakano, T. Uto, D. Adachi, M. Kanematsu & H. Uzu, *Nature Energy* 2 (2017) 17032.

[32]S. Y. Herasimenka, W. J. Dauksher, M. Boccard & S. Bowden, *Solar Energy Materials & Solar Cells* 158 (2016) 98-101.

Vitae:

Weiliang Wu received his Ph.D. degree in physics from Sun Yat-sen University (SYSU), China, in 2018. He focused on the development of high-efficiency dopant-free silicon solar cells in the institute for solar energy systems of SYSU in China. From 2017 to 2018, he was a PhD visiting student in EPFL-PVLAB, Switzerland, working on the dopant-free multilayer back contact (MLBC) silicon solar cells. After Stays at SYSU and EPFL, he became the technical director of process department of Jiangsu Runergy-Yueda PV Technology Co., Ltd, China.

Wenjie Lin received the Bachelor degree in South China Normal University, in 2016. He is currently a Doctoral candidate that involves postgraduate and doctoral study in Institute for Solar Energy Systems, School of Physics, Sun Yat-sen University. He majored in silicon heterojunction solar cells. His research focused on the dopant-free carrier selective contact for highly-efficient silicon solar cell with the low-temperature and simple methods during the fabrication. He developed a novel hole-selective contact material Chromium trioxide (CrO_x), which was successfully applied in silicon based solar cell.

Sihua Zhong received his Ph.D degree in School of Physics and Astronomy from Shanghai Jiao Tong University in 2015. After being a postdoc in Institute of Solar Energy, Shanghai Jiao Tong University for 2 years (2015-2017), he currently do his postdoctoral work in PV-Lab, École Polytechnique Fédérale de Lausanne (EPFL). His research interests focus on novel and highly efficient crystalline silicon solar cells.

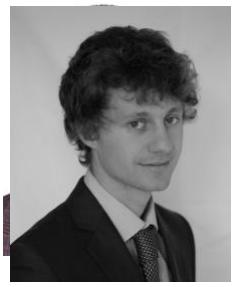

Bertrand Paviet-Salomon was born in Lyon, France, in 1986. He received the M.Sc. degree and the Engineer Diploma degree in theoretical and applied optics, both in 2009, from the Institut d'Optique, Paris, France. From 2009 to 2012, he pursued the Ph.D. degree with the French National Institute for Solar Energy, Le Bourget-du-Lac, France, working on laser processes for crystalline silicon solar cells. He received the Ph.D. degree in electronics and photonics from the University of Strasbourg, Strasbourg, France, in 2012. From 2012 to 2014, he was a Postdoctoral Researcher with the Photovoltaics and Thin-Film Electronics Laboratory, École Polytechnique Fédérale de Lausanne, Neuchâtel, Switzerland, working on high-efficiency back-contacted silicon heterojunction solar cells. In 2014, he joined the PV-Center, Centre Suisse d'Électronique et de Microtechnique, Neuchâtel. His research interests include the development of high-efficiency crystalline silicon solar cells and modules.

Matthieu Despeisse is section head in CSEM PV-center, Neuchâtel, Switzerland, leading the research on silicon heterojunction, passivating contacts, tandem cells, metallization-interconnection and metrology. He received his degree in electrical engineering from INSA, France, in 2002. He then worked until 2008 at CERN in Geneva, Switzerland, focusing on novel Silicon radiation sensors, advanced low-power electronics and technology transfer, where he obtained his PhD in 2006. He joined the PV-lab of EPFL in 2009 in the group of Pr. Ballif, leading the team working on thin film silicon photovoltaics technologies. In 2013, he started the crystalline silicon and metallization activities in CSEM.

Quentin Jeangros received a PhD in Materials Science in 2014 from the Industrial Energy Systems Laboratory of EPFL (collaboration with the Technical University of Denmark). Since the end of 2017, he has been responsible for the Pervoskite Cells for Tandem Applications activities at EPFL PV-Lab. His research activities focus on the use and development of advanced characterisation methods to understand and optimized the nanostructure of materials for energy conversion (solid oxide fuel cells, solar cells), with the aim of improving their efficiency and durability.

Zongcun Liang received his Master degree from institute of coal chemistry, Chinese academy of Sciences (CAS) in 1997, he worked at Guangzhou institute of Energy Conversion, CAS, for the Si thin film solar cells. He got his Ph.D degree from Sun Yat-sen university in 2004, and worked at school of physics, Sun Yat-sen university as an associate professor in 2006 as well as professor in 2016. His current research areas: High-efficiency crystal silicon solar cell; Silicon based heterojunction solar cells; photovoltaic materials.

Hui Shen received his B.S. degree from the Nanjing University of Science and Technology in 1982. From 1992 to 1996, he worked on the nano-scale alloy at the Fraunhofer Institute of Applied

Materials of Germany, as a Ph.D candidate in the Dresden University of Technology for the doctorate degree in material science. From 1997 to 1998, he worked at the South China University of Technology on the nano-materials. From 1999 to 2004, he led a photovoltaic research team in the fields of solar thermal conversion material and silicon thin film solar cell in the Chinese Academy of Sciences. In August of 2004, he founded the Institute for Solar Energy Systems at Sun Yat-sen University (SYSU) and led the team ever since. His current research interest field covers: the physics of a solar cell, solar cell technology and PV application.

Mathieu Boccard received his PhD in Material Science from Ecole Polytechnique Federale de Lausanne (EPFL), PVlab in 2012 on the topic of thin-film-silicon tandem solar cells. He joined the Holman Research Group in Arizona State University from 2014 to 2016 for a postdoc where he worked on high-efficiency crystalline silicon solar cells, carrier-selective contacts for various photovoltaics technologies, and crystalline-silicon-based tandem solar cells. Since 2017, he is leading the silicon heterojunction team in EPFL, PVlab, working on improving the understanding and realization of carrier-selective contacts.

Christophe Ballif received his Ph.D. degree in physics from EPFL, Switzerland, in 1998. After Stays at NREL, Fraunhofer ISE and EMPA, he became in 2004 Full Professor with the Institute of microengineering, University of Neuchâtel, Switzerland, directing the Photovoltaics and Thin-Film Electronics Laboratory, now part of EPFL. Since 2013, he has also been the Director of the PV-Center within CSEM, Neuchâtel, an RTO specialized in industrial research and technology transfer. He has contributed to numerous innovations and products and his current research interests include materials for PV, high-efficiency c-Si solar cells and multijunction, module technology, BIPV, and Energy systems. He received the Becquerel award in 2016.

Supplementary information to:

Dopant-free back contacted silicon solar cells with an efficiency of 22.1%

Weiliang Wu[1,2], Wenjie Lin[1], Sihua Zhong[2], Bertrand Paviet-Salomon[3], Matthieu Despeisse,[3] Quentin Jeangros[2], Zongcun Liang[1,4], Hui Shen*[1,4], Mathieu Boccard*[2] and Christophe Ballif[2,3]

[1] Institute for Solar Energy Systems, School of Physics and State Key Laboratory of Optoelectronic Materials and Technologies, Sun Yat-Sen University (SYSU), Guangzhou, China.

[2] Photovoltaics and Thin Film Electronics Laboratory, Institute of Microengineering, École Polytechnique Fédérale de Lausanne (EPFL), Rue de la Maladière 71b, CH-2000 Neuchâtel, Switzerland.

[3] Centre Suisse d'Électronique et de Microtechnique (CSEM), PV-Center, Rue Jaquet-Droz 1, CH-2002 Neuchâtel, Switzerland.

[4] Shunde-SYSU Institute for Solar Energy, Shunde, China .

*Corresponding author:

1. Hui Shen

E-mail: shenhui1956@163.com;

2. Mathieu Boccard

E-mail: mathieu.boccard@epfl.ch

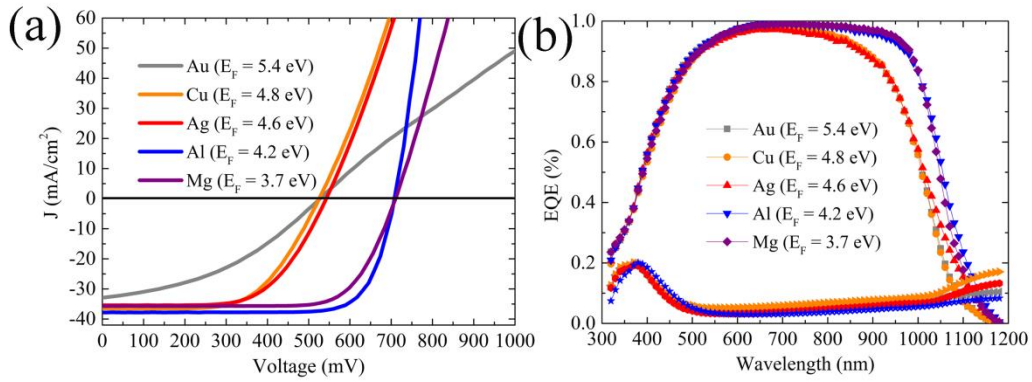

Supplementary Figure 1. Electrical and optical performance influenced by the work-function of contact metals. a, Light current density-voltage (*J-V*) curve of front junction solar cells changed with the work-function (W_F). **b,** External quantum efficiency (*EQE*) is as a function of metal's work-function.

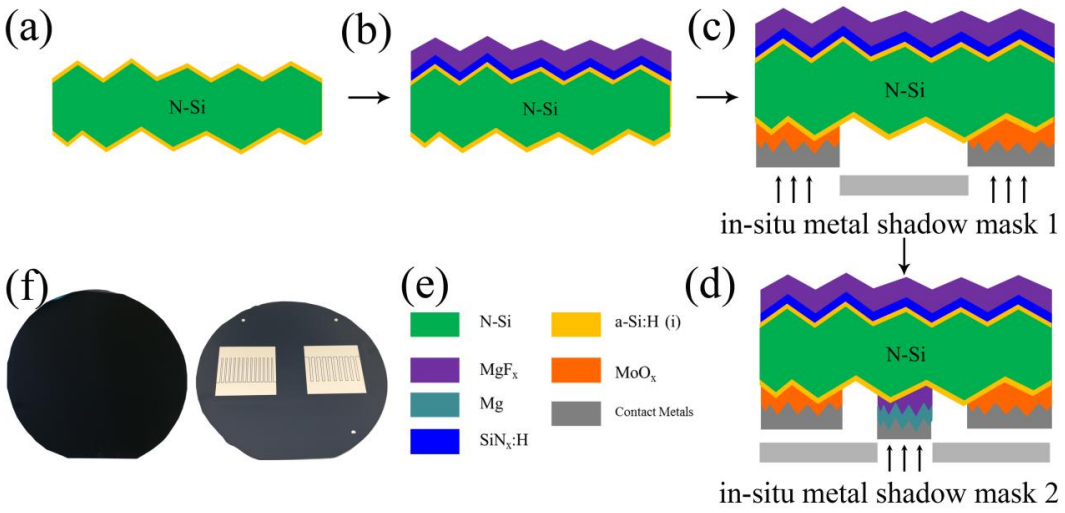

Supplementary Figure 2. Process charts and optical image of dopant-free MLBC solar cells. a, Wet-chemical textured wafer passivation with bifacial a-Si:H(i) films. **b,** MgF_x/SiN_x as ARC deposition at the front. **c,d** Patterned MoO_x/Ag and MgF_x/Mg/Al/Ag films deposition via in situ shadow masking. **e,** The contacting scheme of the MLBC

The obvious effect of W_F on the front junction silicon solar cells performance is shown in

Supplementary Fig. 1. The *J-V* curves were measured under STC, however, are very different than that of cells with good FF and Type I "S" shape cells. The *J-V* curve of Au covering on Mg surface with shows the "S" shape, which arises from an opposing diode or Schottky barrier as can be seen in HIT solar cells with poor back metal contacts. It is shown in Fig. 1b that for Au, Cu and Ag an excellent rear side reflection is observed. In the case of *EQE* represents only those entering the silicon solar cells are counted, which is influenced by the optical performance and effective surface recombination rate on the rear surface responsible for the spectral response in the long wavelength region.

The main challenge of IBC solar cell is the design of the doping and patterning contact on the rear side surface. Moreover, the selective diffusion of boron and phosphorus dopants to achieve low recombination and contact resistivity, the diffusion barriers were required. The SiO_2 film at the backside of the substrate is patterned by the photolithography and SiO_2 etch-back process to keep the local passivation and contact, as well as the metallization design, has to be considered. Thus, conventional processes for IBC solar cells are complex and faced with the high processing costs. Supplementary Fig. 2 shows the approach of patterning of the electron and hole selective contacts, as well as the metallization can be achieved without breaking the vacuum with adding more evaporated boats in the equipment, which enabling a simple fabrication process with only two in situ shadow masking without photolithography patterning steps and two single alignments.

We measured the $i\text{-}V_{oc}$ of the samples of 7.5 nm a-Si:H (i)/c-Si (n)/ x nm a-Si:H (i) with different rear side a-Si:H (i) layer thicknesses, in order to determine effects of a-Si:H (i) layer thicknesses on the a-Si:H (i)/MgFx/Mg/Al electron selective contact performance of MLBC solar cells (see Supplementary Figure 3). We compared $i\text{-}V_{oc}$ of the asymmetric samples, the SiN_x:H can improve the passivation of front surface. As shown in Supplementary Table 1, with increasing a-Si:H (i) layer thicknesses from 5 nm to 10 nm, the V_{OC} increases up to from 688 mV to 720 mV due to better passivation on rear surface, while, the *FF* decreases from 73.0% to 70.5% due to the low conductivity of a-Si:H (i) film. As shown in Supplementary Figure 4, the electron selective contact recombination and ρ_c are increased with the thickness of MgF_x. A range of f_{HTL} from 55 to 60% is also studied in order to know the influence of cell geometry on series resistance and rear surface passivation and its impact on photovoltaic efficiency. From variations of the solar cell performance with the a-Si:H (i), MgF_x layer thicknesses and f_{HTL}, the optimum thicknesses were determined to

be 7.5 nm, 1.5 nm and 55%, respectively.

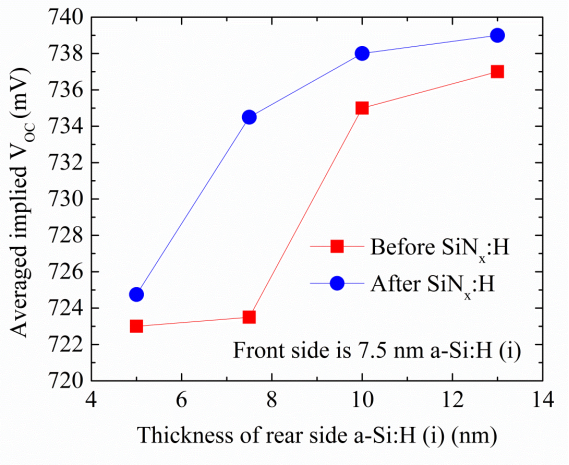

Supplementary Figure 3. The implied-V_{oc} (i-V_{oc}) values are as a function of the different rear-side thicknesses of a-Si:H (i) film.

Supplementary Table 1. Effect of a-Si:H (i) thickness and hole selective contact fraction (f_{HTL}) on MLBC solar cell.

a-Si (i) thickness (nm)	f_{HTL}**(%)**	V_{oc}**(mV)**	J_{sc}**(mA/cm^2)**	***FF* (%)**	***Eff.* (%)**
5	60	638	33.4	72.0	15.3
	55	688	39.0	73.0	19.6
7.5	60	706	38.4	76.2	20.7
	55	718	41.5	74.2	22.1
10	60	715	41.5	70.0	20.8
	55	720	41.6	70.5	21.1

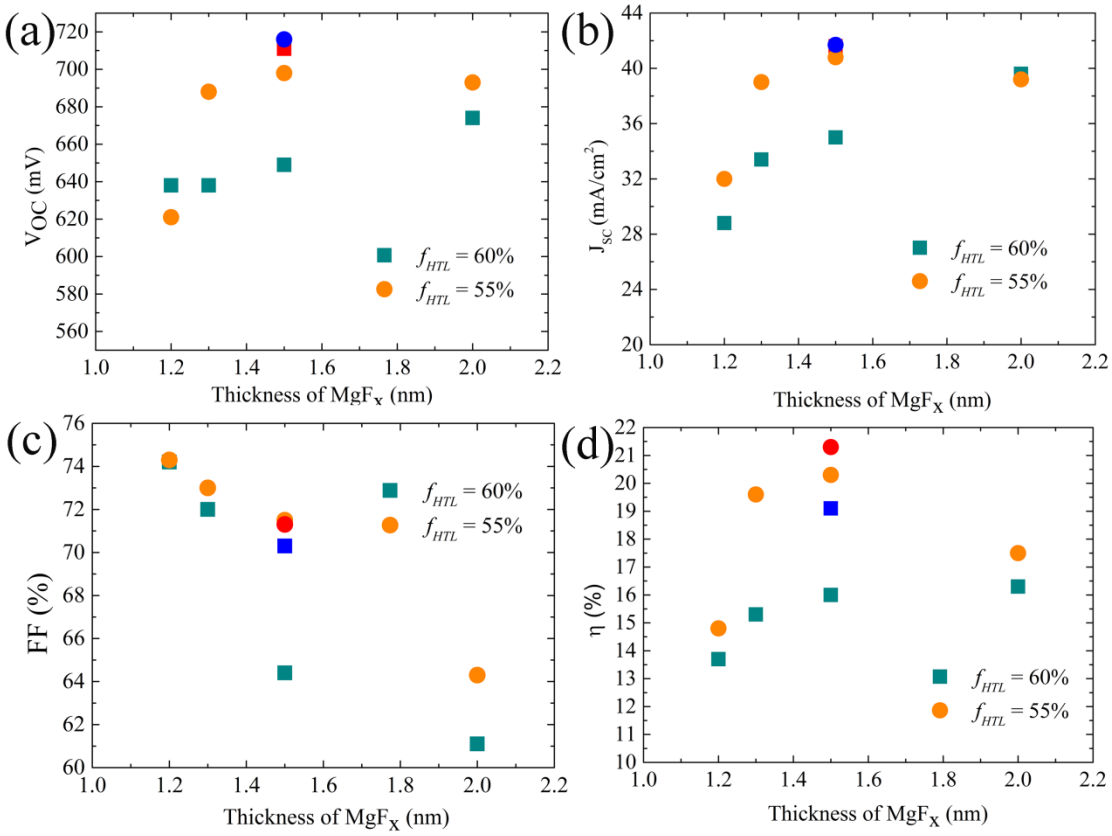

Supplementary Figure 4. The influence of MgF_x thickness on the MLBC solar cells.

The c-Si(n)/a-Si:H (i)/MgF_x/Mg/Al electron-selective contacts were fabricated on textured Fz wafers. The native oxide of c-Si(n)/a-Si:H (i) was removed by the diluted 1% HF dip prior to deposition of MgF_x/Mg/Al films. The eight circular pads with different diameters were evaporated on the c-Si(n)/a-Si:H (i) surface via a metal shadow mask, and the full rear-area was evaporated with 20 nm Mg/100 nm Al. Current-voltage (*I-V*) measurements were taken at room temperature using a 2601 sourcemeter. The resistance versus diameter trend was fitted with a spreading resistance model, allowing accurate extraction of contact resistance ρ_c of 80 mΩcm^2. The pseudo *J-V* curve was also measured and shown in Supplementary Figure 6 indicating a diode characteristic without shunt. Due to the thin Ag (800 nm) of IBC solar cell, series resistance is still large, causing relatively low *FF*. The pseudo *FF* (*pFF: FF* excluding R_S power loss) of 84.2% and pseudo efficiency (efficiency excluding R_S power loss) of 25% are measured.

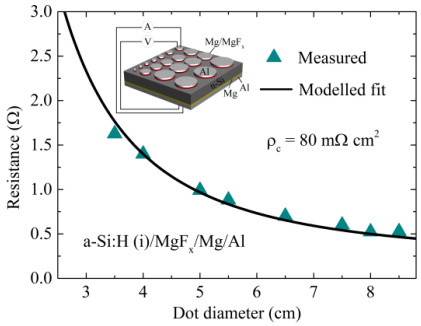

Supplementary Figure 5. Contact resistivity structure and measurement. Contact resistivity extraction of a a-Si:H (i)/MgF_x/Mg/Al contact to c-Si (n). The insert is the schematic of the ρ_c test structure.

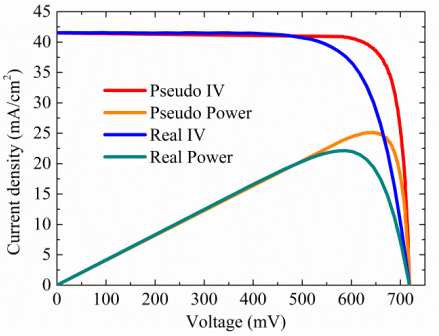

Supplementary Figure 6. Influence of series resistance based on the pseudo *J-V* curve from *Suns-*V_{OC} and the real *J-V* curve of the MLBC solar cell.

Supplementary Table 2. State-of-the-art of dopant-free silicon solar cells measured under STC.

Institute	Hole contact	Electron contact	A (cm^2)	V_{oc} (mV)	J_{sc} (mA/cm^2)	FF (%)	η (%)
SYSU& EPFL	MoO_x	MgF_x/Mg/Al	4.5	718	41.5	74.2	22.1
UCB & ANU & EPFL	MoO_x	TiO_2/LiF_x/Al	4	706	38.4	76.2	20.7